APPLICATION OF MACHINE LEARNING TECHNIQUE FOR MAPPING RAYED CRATERS, RILLES AND RIDGES ON THE MOON. Y. Daket[1] (daket-y@u-aizu.ac.jp), C. Honda[1], and H. Demura[1], 1The University of Aizu, Aizu Research Center for Space Informatics, Aizu-Wakamatsu, Fukushima 965-8580, Japan.

Introduction: Recently, more and more planetary surface images are obtained. To process and analyze them efficiently, automatic data processing is important. Application of machine learning techniques will be one of the solutions.

In this study, we focused on making geological map of the Moon by using a machine learning technique. Geological maps are used for i.e. understanding evolution of lunar surface, investigating subsurface composition and structures, and selecting landing site. Geologic maps are integration of multiple thematic maps such as a map of surface compositional features and tectonic structures etc. We applied a machine learning technique to make a thematic map containing rayed craters, rilles and ridges.

Data: Visible and near-infrared images obtained by Terrain Camera (TC) and Multiband Imagers (MI) were employed. TC and MI were onboard SELENE. Spatial resolution of TC and MI images are ~10 m/pix [1] and ~20 ~60 m/pix [2], respectively. Additionally, we used topography data, Digital Terrain Model (DTM) calculated from TC images [1], were employed. Spatial resolution of DTM is ~10 m/pix. TC observed lunar surface with visible range. MI observed lunar surface in 9 different channels whose wavelength range from 415 to 1055 nm. These images are advantageous to perform global survey in same quality, because they cover the entire lunar surface in same resolution and same solar condition.

Study area and Method: The region of south Sinus Medii (3x3 degrees in size) was chosen for the training, validating, and testing fields (Figure 1). The area is located on the nearside mare covered by basalts. A several grabens, sinuous rilles, mare ridges, and numerous craters are observed. Bright green and bright blue circles appeared in the figure, are rayed craters. The bright plain surrounding rayed craters are their ejecta. The horizontal extents of ejecta vary depending on the craters; some have elliptical shape, and some have radial pattern.

We implemented mostly after the semantic segmentation architecture, called Efficient Neural Network (Enet) [3], but we employed different activation function called Funnel Activation (FReLU) [4] instead of PReLU. ENet is a deep neural network architecture for semantic segmentation. It requires low real time inference in comparison to other deep neutral networks.

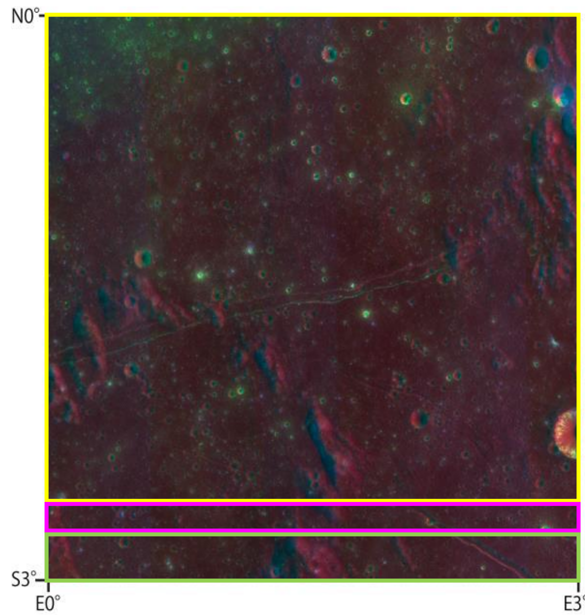

Figure 1: Composed image (Image Type A) of south of Sinus Medii. Yellow, pink and green squares show the regions for training, test and validation, respectively.

FReLU is capable of considering 2D spatial condition. By using FReLU, higher detection capability of linear features is expected.

We made two kind of composite images as for the training, validation, and test data. One is made of TC and MI images (Image Type A; Figures 1, 2a, 3a) and the other is made of DTM and MI images (Image Type B).

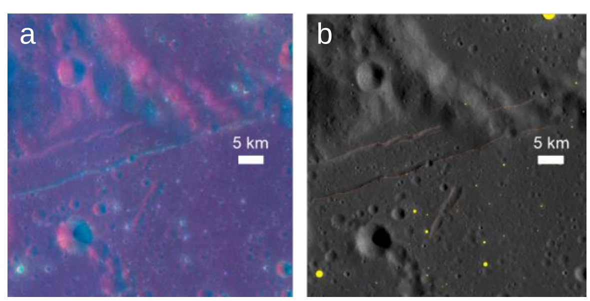

Figure 2: (a) close up image of Image Type A (displayed color range is different from Figure 1), and (b) TC image with manually labeled craters (yellow circles) and faults (brown solid lines).

The lunar surface spectral features vary due to the difference in composition and amount of space weathering. Ejecta exposed by rayed craters are not space weathered, thus they show different spectral features from the surrounding area. Also young craters have sharper topographic features than old ones. Accordingly, visible and near-infrared images and topography information make it easier to recognize rayed craters.

Image Type A is a composed of TC image as red, MI band ratio image of 749 nm/1001 nm as green, MI band ratio image of 414 nm/749 nm as blue. Image Type B is a composed image of slope map (calculated from DTM) as red, MI band ratio image of 749 nm/1001 nm as green, MI band ratio image of 414 nm/749 nm as blue.

In advance, to adjust the spatial resolution gap between TC and MI images, MI images were artificially interpolated and set to the resolution of 10 m/pix by nearest neighbor.

We also manually prepared labeled images that have three classes, “rayed craters”, “fault”, and “others” (Figure 2). There are more than ~2000 craters larger than 100 m in diameter in the study area. Several rilles and ridges are distributed.

The composite and labeled images were divided into 576 pieces, 512x512 pixels size each. Among them 504 images were used for training. 48 images were used for validation, and 24 images were used to test and evaluate trained models. We set the batch size of 14. We continued learning until epoch number of 2000, then we adopted the best model among them. We used Intersection over Union (IoU) metric to evaluate trained models.

Results: Rayed craters (being larger than ~70 m and smaller than ~1 km in diameter) predicted by the trained model meet good agreement with the manually extracted craters (Figure 3). Some clear rilles were extracted very well, but other ambiguous rilles and ridges were not well extracted.

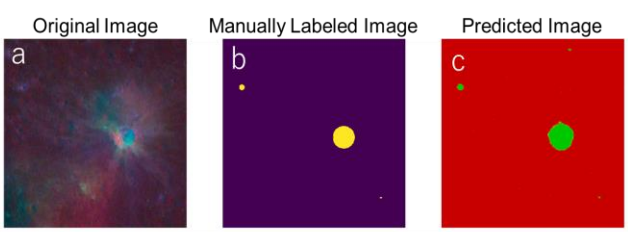

Figure 3: Example showing (a) input image (Image Type A), (b) manually labeled image (craters as yellow), and (c) predicted image (craters as green) by the optimal trained model.

The trained model applied to Mare Imbrium region (Figure 4). As you can see in the figure, rayed craters are well detected and ridges are partially detected.

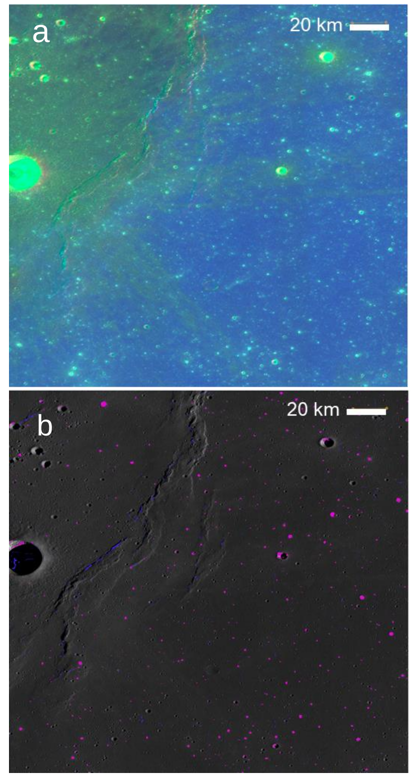

Figure 4: Part of Mare Imbrium region. (a) input image (Image Type A) and (b) TC image with predicted craters (pink) and faults (blue).

Discussion and Conclusion: The reason why small craters (D<~70 m) were not extracted well is explained by the spatial resolution. Their dimeters are close to detection limit, because spatial resolution of MI image is ~60 m/pix.

Low detection capability of large craters (D>~1 km) and fault features would be explained by lack of supervised images. There were only ~10 rayed craters larger than 1 km. We consider that the small training data set for fault features result in those low detection. We expected by using topography information would be resolve this problem, but dataset of Image Type B did not improve detection ability. The extractions of those features are remained for future work.

References: [1] J. Haruyama, T. Matsunaga, M. Ohtake (2008), Earth Planet Sp., 60, 243—255. [2] M. Ohtake, J. Haruyama, T. Matsunaga, S. Kodama, T. Morota, Y. Yokota (2008), Advances in Space Research, 42, 301—304. [3] A. Paszke, A. Chaurasia, S. Kim, E. Culurciello (2016), arXiv preprent. [4] N. Ma, X. Zhang, and J. Sun (2020), arXiv eprent 2007.11824.